Letter

Convection of monodisperse particles in a highly filled rotating cylinder

Shoichi Yoneta, Hiroyuki Ebata, and Shio Inagaki
Department of Physics, Graduate School of Science, Kyushu University, Fukuoka 819-0395, Japan

(Received 11 October 2023; accepted 18 December 2023; published 2 February 2024)

We investigate the occurrence of spontaneous convection in a coaxial cylinder highly filled with monodisperse spheres. To analyze the flow field noninvasively, initial pulses consisting of colored particles are placed at equal intervals. By analyzing the spatiotemporal distribution of these pulses, we obtained axial velocity profiles for both the surface and subsurface regions. Our advection-diffusion equations with steady advection terms incorporate experimentally obtained axial velocity profiles in the surface layer, while the rest of the components are estimated using azimuthal symmetry and volume conservation. The validity of our model is confirmed by comparing experimental data with numerical solutions for both the spatiotemporal distribution and cross-sectional profile of the colored particles.

DOI: 10.1103/PhysRevE.109.L022901

Granular materials exhibit a rich range of behaviors, including melting, flowing, and even boiling, in response to applied mechanical agitation [1]. Unlike traditional states of matter such as solid, liquid, or gas, granular materials defy simple classification due to the dissipative interactions between their constituent particles. Granular flow has been extensively studied as it is widely found in both nature and industrial processes [2–4].

Granular materials exhibit a fascinating property of segregation when subjected to mechanical agitation, such as rotation and vibration [5]. When a cylinder is highly filled with a bidisperse granular mixture and rotated horizontally, a segregated pattern emerges as the particles flow down the surface [6]. One may expect that the bulk under the fluidized region would be frozen where geometrical restrictions prevent the independent motion of the particles. However, granular materials can flow collectively over extended time scales [7]. Reflecting this highly viscous fluid-like nature, very slow three-dimensional convective motion has also been observed in such highly filled bidisperse systems [6,8,9]. In the case of a coaxial cylinder, the segregated pattern moves either in one direction or oscillatively, depending on the slight change in the fill level [10]. Rietz and Stannarius also observed convection rolls in horizontally rotating cells [11]. One question might arise here as to whether the motion of the segregated pattern is originated from the rearrangements caused by the segregation or whether a confined system filled with discrete particles can spontaneously form collective motion, such as convection. From a process engineering perspective, it is also essential to understand the collective behavior of granular materials.

To investigate the collective behavior of densely packed granular media, we conducted experiments using monodisperse spheres in a rotating coaxial cylinder, demonstrating global convection alongside diffusion. The setup consisted of an acrylic coaxial cylinder with inner and outer radii, r_i and r_s, measuring 20 and 40 mm, respectively, and a length L of 345 mm. To facilitate cross-sectional observation, the cylinder was divided into two semicircular sections and securely fastened together, allowing for separation after rotation [12]. We used spherical alumina beads (280 ± 70 μm, density g/cm^3). To visualize the flow field, we used white and red particles. The red particles were colored with oil-based magic ink. The effect of coloration on particle behavior is discussed in Supplemental Material Sec. B, where no considerable impact was observed [12]. We placed the cylinder vertically, and poured alternately white and colored particles into the cylinder to achieve a fill level of 95%. The fill level is defined as the fraction of the total volume of the cylinder occupied by all particles and voids between them. The cylinder was placed on parallel shafts and rotated at 15 rpm using a brushless dc electric motor (Oriental Motors).

To capture the overall picture of the flow, we carried out an experiment with seven colored pulses placed at equal intervals in the initial state [Fig. 1(a)]. The cylinder was rotated for 5 h. The images are grayscaled for analysis. Figure 1(b) shows the spatiotemporal diagram of the surface flow field, created by stacking one-pixel-high horizontal lines of the images taken every 30 s. The diagram exhibits distinct trajectories of the seven pulses, originating from the initial position and extending towards both end walls. This observation strongly suggests the occurrence of flow from the center to the end walls on the surface of the cylinder. Remarkably, additional blurred trajectories were observed originating from the initial position of the pulses and extending towards the center of the cylinder, counter to the predominant motion of the prominent pulses.

Figure 1(c) is one of the two cross sections obtained after rotating the coaxial cylinder for 5 h. The upper and lower sides of the rectangular cross section corresponds to the outer and inner cylinder. In the central region, the seven pulses of colored particles remained vertically aligned, indicating that the axial velocity in this region is independent of the radial direction. At the boundary of the inner cylinder, slip occurs, suggesting plug flow characteristics similar to Bingham fluids that exhibit yield stress. The intervals between the pulses remain nearly equal but narrower than the initial configuration. Furthermore, there is a one-to-one correspondence between the position of the colored pulses of the cross section and the

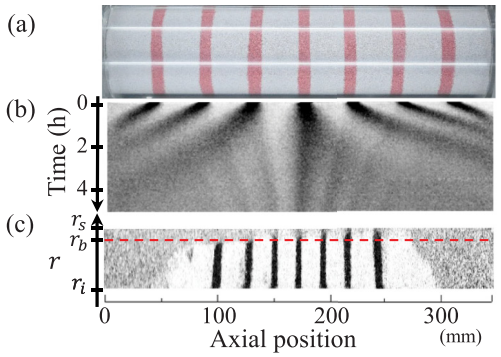

FIG. 1. (a) Initial configuration with seven colored pulses with a fill level of 95%. (b) Spatio-temporal diagram of the surface pattern. (c) Cross-sectional image after 5 hours of rotation. The aspect ratio of the image is increased by 2.8 vertically for ease of viewing.

final position of the blurred trajectories on the spatiotemporal diagram. It indicates that the blurred trajectories are colored particles that exude from the subsurface. The time evolution of the positions of the colored pulses in the subsurface region was detected in a noninvasive manner by tracking the blurred trajectories.

Based on the cross-sectional image in Fig. 1(c), we delineate two distinct layers within the system: a surface layer characterized by particles traversing the fluidized region under rotation, and an inner layer where particles exhibit collective bulk movement. In our previous experiment with a bidisperse particle system in a rotating coaxial cylinder [10], we distinctly observed a boundary between the outer and inner layers parallel to the axis. Utilizing this observation, we defined the boundary between the inner and outer layers, as illustrated in Fig. 1(c). We assume the thickness of the outer layer is constant irrespective of the axial position, which is determined by the thickness of the mixed domain near the center of the cylinder. Although the mixed regions were formed at both ends of the inner layer, it is due to the colored particles entering the inner layer at the ends of the cylinder and flowing back towards the center. Figure 2(a) demonstrates the time evolution of the gray-scale intensity values around the second pulse from the left in the spatiotemporal diagram in Fig. 1(b). The pulse center moves leftward and its width increases progressively. This behavior is consistent among the other six pulses, indicating symmetry at the cylinder's center. The observations suggest an advection flow from the center to the end walls, accompanied by particle diffusion. The intensity of each pulse is fitted with a Gaussian distribution, and its variance, representing the pulse width, is plotted against time in Fig. 2(b). The thick line represents the average variance. By assuming one-dimensional normal diffusion, the axial diffusion coefficient is estimated to be approximately 82 mm^2/h. It should be noted that in a half-filled monodisperse system, the normal diffusion in the axial direction was also observed numerically [15]. The axial velocities in the inner and surface layers were determined by analyzing the time evolution of the pulse centers in the spatiotemporal diagram, where the pulse intensities were fitted with a Gaussian distribution [Fig. 2(c)]. The overlapping velocities among the pulses indicate position-dependent velocity distribution. The axial velocity distribution is not entirely symmetric along the axis

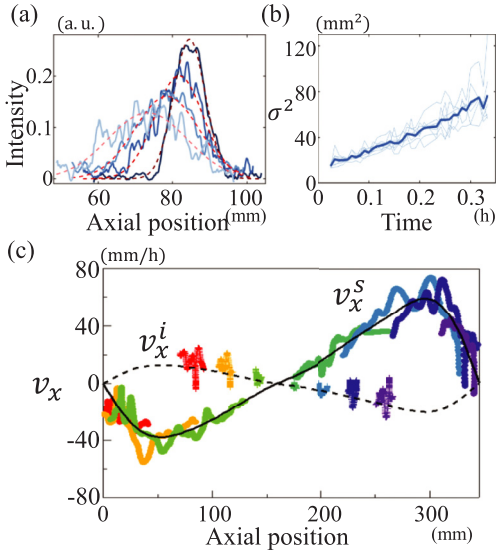

FIG. 2. (a) Intensity of the pixels around the second pulse from the left in the spatiotemporal diagram at time $t = 3, 11, 19,$ and 26 min from dark blue to light blue. Dashed lines denote the Gaussian fitting curves. (b) Variance of the Gaussian fitting of the brightness (light blue: seven individual pulses, dark blue: average of seven pulses). (c) Axial velocity profiles in the surface (o) and inner (*) layers. Solid line: the fitting curve of v_x^s. Dashed line: the estimated axial velocity in the inner layer. The pulses from left to right corresponds to the data with colors from red to purple.

due to initial container-filling procedures. Despite efforts to achieve uniform density by meticulous filling and consistent positioning, asymmetry persists. We consistently positioned the prior bottom-facing section to the left during rotation. Therefore, the convective phenomenon exhibited consistently high reproducibility.

We propose an advection-diffusion model considering both advective motion and diffusive behavior in our system. Using cylindrical coordinates (r, θ, x), where x is the axial position from the left end of the cylinder, r is the radial distance from the x axis, and θ is the azimuthal angle, we assume symmetry with respect to θ despite the presence of a narrow avalanche along the axis. Additionally, we consider that the colored particles follow the velocity field without influencing it, making the total particle system's velocity equivalent to that of the colored particle component. By combining the assumption of incompressibility and axial symmetry, along with the law of conservation of mass, we can derive the advection diffusion equation in terms of the concentration of the colored particles, ϕ_A, which is defined as the ratio of the density of the colored particles to the density of the total particle system as follows:

$$\frac{\partial \phi_A}{\partial t} + v_x^\alpha \frac{\partial \phi_A}{\partial x} + v_r^\alpha \frac{\partial \phi_A}{\partial r} = \frac{1}{r}\frac{\partial}{\partial r}\left[D_r^\alpha r \frac{\partial \phi_A}{\partial r}\right] + D_x^\alpha \frac{\partial^2 \phi_A}{\partial x^2}, \quad (1)$$

where the diffusion coefficients in axial and radial directions are presented by D_x^α and D_r^α, while the axial and radial velocities within the total particle system are denoted as v_x^α and v_r^α, respectively. The superscript letter α represents i for the

inner layer and s for the surface layer. Within the inner layer, characterized by densely packed particles, their collective interactions prevent independent motion. As a result, we assume zero diffusion coefficients, D_x^i and D_r^i, for the inner layer, reflecting the restricted particle mobility. The comprehensive derivation is given in Supplemental Material Sec. C [12]. To solve these equations numerically, the diffusion coefficients and steady advection terms are required. First, the axial velocity in the surface layer, v_x^s, was fitted to the experimental data using the following function:

$$v_x^s = \sum_{k=1}^{4} [A_k \sin 2k\pi\tilde{x} + B_k \cos(2k-1)\pi\tilde{x}], \tag{2}$$

where $\tilde{x} = x/L - 1/2$. The detailed values of A_k and B_k are listed in Supplemental Material Sec. D [12]. The fitting function is plotted by a solid line in Fig. 2(c). In the surface layer, which is approximately 13 diameters thick, we approximate the axial velocity at any r using the representative surface velocity. In the inner layer, since the flow behaves in a plug-flow manner as observed in Fig. 1(c), we assume that the axial velocity is independent of r. Second, the axial velocity in the inner layer is derived from that in the surface layer. Incompressibility implies constant density and no inflow or outflow in the system. Therefore, the net flux through any cross section must be zero. Given these conditions, v_x^i and v_x^s must satisfy the relation $\pi(r_b^2 - r_i^2)v_x^i + \pi(r_s^2 - r_b^2)v_x^s = 0$. The radial position of the layer boundary, r_b, is set at 3.6 mm, determined from the cross-sectional image in Fig. 1(c). Consequently, the axial velocity in the inner layer, v_x^i, can be derived from the axial velocity in the surface layer, v_x^s, as

$$v_x^i = -\frac{r_s^2 - r_b^2}{r_b^2 - r_i^2} v_x^s. \tag{3}$$

The estimated v_x^i is represented by the dashed line in Fig. 2(c), which shows a good agreement with the experimental data.

In terms of the radial velocity profiles, based on the assumption of incompressibility and axial symmetry and the law of conservation of mass, the inflow and outflow of particles in the axial direction must be balanced with that in the radial direction. As a result, the radial velocity distributions in the inner and surface layers, v_r^i and v_r^s, can be written as

$$v_r^\alpha(x, r) = \frac{{r_\alpha}^2 - r^2}{2r} \frac{dv_x^\alpha(x)}{dx}, \quad (\alpha = i, s). \tag{4}$$

See Supplemental Material Sec. E [12] for details of the derivation. By substituting Eqs. (2) and (3) into Eq. (4), we can estimate the radial velocity profile in the surface and inner layers. It should be noted that the radial velocity v_r^α depends on both r and x. The radial velocity profile $v_r^i(x, r = r_b)$ is depicted in Fig. 3(a). By utilizing the experimentally obtained v_x^s, we derive the analytical expressions for the remaining components, v_x^i, v_r^s, and v_r^i, by employing the principles of volume conservation and axial symmetry. Based on the overall velocity profiles shown in Figs. 2(c) and 3(b), the stream line is depicted with a heat map. We inferred the presence of a two-vortex internal structure. Specifically, the right half exhibits a clockwise vortex, while the left half exhibits a counterclockwise vortex.

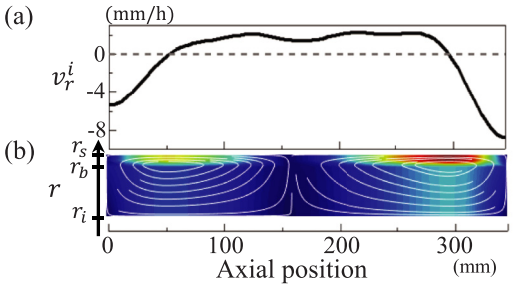

FIG. 3. (a) Estimated radial velocity profile $v_r^i(x, r = r_b)$ derived from Eq. (3). (b) Stream line with heat map. The aspect ratio is increased by 2.8 vertically for ease of viewing.

To validate the advection-diffusion equations in Eq. (1), we numerically solved them by using an explicit finite difference method. See Supplemental Material Sec. F [12] for details of the numerical simulation. The diffusion coefficients in axial and radial directions in the surface layer, D_x^s and D_r^s, were set at 30 and 6 mm^2/h, respectively. To achieve consistency between the numerical solution and experimental data, the diffusion coefficient in the surface layer, D_x^s, was fine-tuned to a lower value than initially derived from the pulse data in Fig. 2(b). Similarly, the radial diffusion coefficient, D_r^s, was selected to better match the spatiotemporal plot and cross section with the experimental results in Figs. 1(b) and 1(c). The effects of altering the radial diffusion coefficient on the numerical computation results of the advection-diffusion equations are detailed in Supplemental Material C [12]. The numerical solution of the advection-diffusion equations described in Eq. (1) is presented in Fig. 4. The spatiotemporal plot successfully reproduces the qualitative characteristics observed in the experiment, such as the clear trajectories in the surface layer and the diffuse trajectories exuding from the inner layer shown in Fig. 1(c). The cross-sectional features in the experiment shown in Fig. 1(c) are also well represented in the numerical solution shown in Fig. 4(b).

When a container is nearly completely filled with a bidisperse granular mixture and rotated horizontally, three-dimensional convective motions were observed [6,8–10]. Our current study shows that in a densely packed granular system, convective motion can occur even without segregation. This suggests that surface flow contributed to the formation of

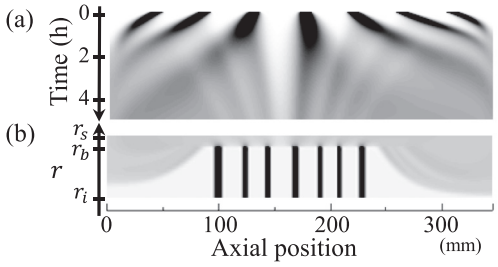

FIG. 4. Numerical solution of the advection-diffusion equation. The color corresponds to the concentration of the colored particles. (a) Spatiotemporal diagram with a duration of 5 h. (b) Cross section. The aspect ratio of the image is increased by 2.8 vertically for ease of viewing.

segregated patterns, while the collective band movement was associated with macroscopic convection. Further experiments are needed to ascertain whether phenomena observed in the bidisperse system, such as oscillatory convection and the splitting of convection rolls, are also present in the monodisperse case when altering the fill level.

In this paper, we have presented an experimental study of granular convection nearly filled in a coaxial cylinder. The densely packed monodisperse system exhibited convective motions in the absence of segregation. We obtained the axial velocity distribution in the inner layer from the trajectories of the pulses in the spatiotemporal diagram. We successfully derived the axial velocity in the inner layer and the radial velocity distributions in both the inner and outer layers from the axial velocity in the surface layer by employing the conservation law and axial symmetry. Using these velocity profiles as steady advection terms, we numerically solved the advection-diffusion equation and successfully reproduced the experimental results. This provides compelling evidence that the trajectories of the blurred pulses capture the flow in the inner layer in a noninvasive manner.

To understand three-dimensional granular flow, various studies have explored methods to visualize internal structures, through both invasive and noninvasive approaches. The simplest invasive method involves opening the container, either with or without solidifying particles, and observing the cross section [6,9,16]. While this method is straightforward and economical in terms of labor and time, it lacks the capability to capture the time evolution of subsurface convective motion. In contrast, noninvasive techniques such as magnetic resonance imaging [17], nuclear magnetic resonance [8], and positron emission particle tracking [18] are effective, although they can incur substantial costs to ensure temporal walls and spatial resolution. Our experiment holds particular significance as it allowed us to visualize the subsurface flow field in a remarkably simple manner.

Our model does not explicitly include parameters characterizing the granular medium. We assume that the physical properties of the media have been included in the advection and diffusion of the flow field and the thickness of the surface avalanche, which are observable quantities. For example, the ratio of particle diameter to the thickness of the coaxial cylinder significantly influences the fluidity of the media and, consequently, the overall flow field. Moreover, the thickness of the surface layer is influenced by various factors, including the particle shape, the fill level, and the rotational speed of the cylinder. However, a deeper understanding of how the velocity profile is determined based on the material properties of the particles requires further experimental studies.

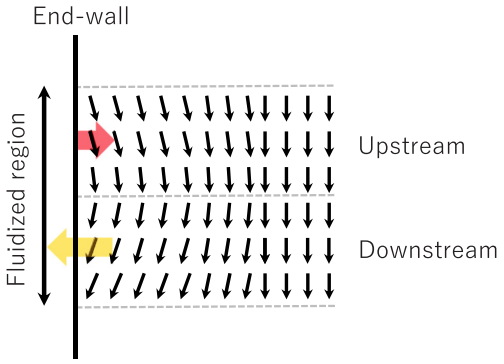

FIG. 5. Schematic picture of the flow field near the end wall.

A fundamental question still remains as to how such a stationary flow field could originally arise by rotation. The sudden drop of v_r^i near the end walls in Fig. 3(a) suggests that friction from the end walls could be a driving force behind the convective motion. Previous experimental [16,19–21] and numerical [22–24] investigations have explored the influence of end walls on the flow dynamics. Pohlman experimentally demonstrated curved streamlines adjacent to the end walls in a half-filled cylinder. These streamlines illustrate particle movement away from the end wall in the upstream direction and a subsequent return toward the end wall in the downstream to ensure mass conservation [19]. Figure 5 depicts this asymmetric axial flow between the upstream and downstream, which emerges as a primary candidate for initiating convection in our system. The greater magnitude of axial velocity in the downstream region than in the upstream results in an overall outward flow along the wall. Subsequently, it must turn radially inwards at the end walls to maintain mass conservation. If this is the case, the length of the cylinder might hold relevance as an additional contributing parameter. As a preliminary investigation, we examined the effect of rotational speed, and the results indicated that higher rotational speeds resulted in faster convection motion, shown in Supplemental Material Sec. G [12]. This observation is consistent with the experimental findings, where the magnitude of axial velocity at the end walls substantially increased with increasing rotation speed [19]. Further research will undoubtedly deepen our comprehension of the underlying mechanisms governing granular convection.

We thank Michio Otsuki for carefully reviewing the manuscript. This work was supported by JSPS KAKENHI Grants No. 22K03468 and No. 22K03552.

[1] H. M. Jaeger, S. R. Nagel, and R. P. Behringer, Rev. Mod. Phys. **68**, 1259 (1996).
[2] G. D. R. MiDi, Eur. Phys. J. E **14**, 341 (2004).
[3] Y. Forterre and O. Pouliquen, Annu. Rev. Fluid Mech. **40**, 1 (2008).
[4] R. M. Iverson, Rev. Geophys. **35**, 245 (1997).
[5] G. Seiden and P. J. Thomas, Rev. Mod. Phys. **83**, 1323 (2011).
[6] S. Inagaki and K. Yoshikawa, Phys. Rev. Lett. **105**, 118001 (2010).
[7] T. S. Komatsu, S. Inagaki, N. Nakagawa, and S. Nasuno, Phys. Rev. Lett. **86**, 1757 (2001).
[8] M. Nakagawa, S. A. Altobelli, A. Caprihan, and E. Fukushima, Chem. Eng. Sci. **52**, 4423 (1997).
[9] H. P. Kuo, P. Y. Shih, and R. C. Hsu, AIChE J. **52**, 2422 (2006).

[10] S. Inagaki, H. Ebata, and K. Yoshikawa, Phys. Rev. E **91**, 010201(R) (2015).
[11] F. Rietz and R. Stannarius, Phys. Rev. Lett. **100**, 078002 (2008); **108**, 118001 (2012).
[12] See Supplemental Material at http://link.aps.org/supplemental/10.1103/PhysRevE.109.L022901 for details of experiment, mathematical derivation of the model, and simulation method. The Supplemental Material also contains Refs. [13,14].
[13] P. Chadwick, *Continuum Mechanics: Concise Theory and Problems* (Dover Publications, New York, 1999).
[14] H. Takewaki and T. Yabe, J. Comput. Phys. **70**, 355 (1987).
[15] N. Taberlet and P. Richard, Phys. Rev. E **73**, 041301 (2006).
[16] A. Santomaso, M. Olivi, and P. Canu, Chem. Eng. Sci. **59**, 3269 (2004).
[17] K. M. Hill, A. Caprihan, and J. Kakalios, Phys. Rev. Lett. **78**, 50 (1997).
[18] Y. L. Ding, J. P. K. Seville, R. Forster, and D. J. Parker, Chem. Eng. Sci. **56**, 1769 (2001).
[19] N. A. Pohlman, J. M. Ottino, and R. M. Lueptow, Phys. Rev. E **74**, 031305 (2006).
[20] A.-N. Huang, L.-C. Liu, and H.-P. Kuo, Powder Technol. **239**, 98 (2013).
[21] J. E. Maneval, K. M. Hill, B. E. Smith, A. Caprihan, and E. Fukushima, Granular Matter **7**, 199 (2005).
[22] P. Chen, J. M. Ottino, and R. M. Lueptow, Phys. Rev. E **78**, 021303 (2008).
[23] U. D'Ortona, N. Thomas, and R. M. Lueptow, Phys. Rev. E **97**, 052904 (2018); **105**, 014901 (2022).
[24] M. M. H. D. Arntz, W. K. den Otter, H. H. Beeftink, R. M. Boom, and W. J. Briels, Granular Matter **15**, 25 (2013).